JACS
JOURNAL OF THE AMERICAN CHEMICAL SOCIETY
pubs.acs.org/JACS
Article

Silver-Exchanged Zeolite Y Catalyzes a Selective Insertion of Carbenes into C−H and O−H Bonds

Yongkun Zheng, Alejandro Vidal-Moya, Juan Carlos Hernández-Garrido, Marta Mon,* and Antonio Leyva-Pérez*

Cite This: J. Am. Chem. Soc. 2023, 145, 24736−24745

ABSTRACT: Commercially available zeolite Y modulates the catalytic activity and selectivity of ultrasmall silver species during the Buchner reaction and the carbene addition to methylene and hydroxyl bonds, by simply exchanging the counter cations of the zeolite framework. The zeolite acts as a macroligand to tune the silver catalytic site, enabling the use of this cheap and recyclable solid catalyst for the in situ formation of carbenes from diazoacetate and selective insertion in different C−H (i.e., cyclohexane) and C−O (i.e., water) bonds. The amount of catalyst in the reaction can be as low as ≤0.1 mol % silver. Besides, this reactivity allows deeply drying the HY zeolite framework by making the strongly adsorbed water molecules react with the in situ formed carbenes.

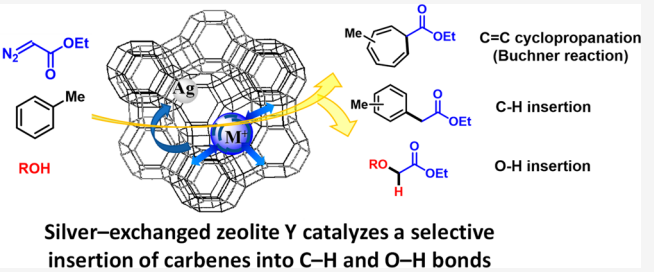

Silver−exchanged zeolite Y catalyzes a selective insertion of carbenes into C−H and O−H bonds

INTRODUCTION

Ag-supported zeolites have been known for decades[1] and found application in diverse fields such as antimicrobial agents,[2] adsorbents of methyl iodide in nuclear power plants,[3] and catalysts for methane activation,[4] 1-butene dimerization,[5] and nitrogen oxides and carbon monoxide redox reactions,[6] among others.[7] However, it is difficult to find in the literature the use of Ag-supported zeolites as catalysts for fine organic synthesis, despite the paramount relevance of Ag as catalyst in many organic transformations.[8,9] The lack of examples with Ag zeolites is due to the tendency of Ag to aggregate inside the zeolite and block the pores, hampering the diffusion and reactivity of molecules composed by more than three or four atoms.[10]

In the past decade, the advent of single-atom catalysts (SACs) has spurred the investigation of solid supports to generate and stabilize SACs on surfaces, with applications in organic synthesis.[11] In this regard, Ag is one of the more interesting chemical elements to be stabilized as a SAC, since its tendency to easily agglomerate, even with just ambient light, has severely hampered the study of the catalytic behavior of single- and few-atoms Ag entities, beyond those prepared by atom deposition or electrochemical techniques.[12] Our group has recently reported the synthesis of Ag dimers (Ag_2) in metal organic frameworks (MOFs) and their use as catalysts for the Buchner reaction,[13a] the oxidation sulfonation of styrenes,[13b] and the methanation of CO_2.[13c] However, single Ag atoms could not be prepared, and the electronics of the catalytically active Ag site were fixed by the MOF surroundings, without any room for catalytic tunability.

Here, we show that the commercially available, robust, and crystalline microporous aluminosilicate zeolite Y stabilizes catalytically active single Ag atoms and subnanometric clusters inside its cavities, after wet exchange with $AgNO_3$ and calcination under air at 450 °C. Figure 1 shows that the

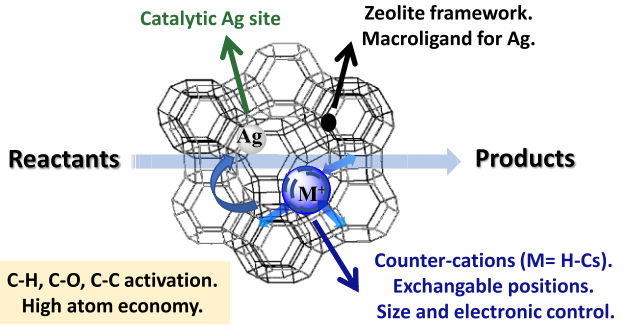

Figure 1. Schematic representation of the strategy employed here to prepare solid-supported Ag atoms in zeolites to be used as selective catalysts for highly efficient organic reactions. When going from H^+ to Cs^+, Ag receives more electron density through the zeolite framework and the steric hindrance in the supercages also increases.

Received: August 2, 2023
Revised: October 18, 2023
Accepted: October 19, 2023
Published: November 3, 2023

https://doi.org/10.1021/jacs.3c08317
J. Am. Chem. Soc. 2023, 145, 24736−24745

charge-compensating cations of the zeolite regulate the electron density on the Ag site.[14] When going from H^+ to Cs^+, the electron density of the framework increases, since the bigger (softer) the counter cation, the higher the electron density on the framework, which is ultimately received by the Ag sites.[15] In other words, a regulated electron flow occurs internally in the zeolite from the counter cation site to the Ag site, since the less electronegative counter cations, i.e. Cs^+, enable more electron density to be received by Ag. If one also considers the difference in size between counter cations, an array of different electronic and steric Ag-supported materials, with potential application in a diversity of organic reactions, is easily obtained.

We will show here that the resulting zeolites catalyze representative carbene-mediated reactions in organic synthesis, such as the Buchner reaction and acetate insertion in methylene and hydroxyl bonds.[16,17] The Ag-zeolite enables the reaction of C−H and C−O bonds without requiring prefunctionalized substrates or leaving groups (such as halides, etc.), and not only the catalytic activity but also the selectivity of the reaction is dictated by the counter cation of the zeolite. To our knowledge, these carbene-mediated reactions are rarely catalyzed by a solid support,[18] and some of them are here catalyzed by Ag for the first time.

RESULTS AND DISCUSSION

1. Synthesis and Characterization of Ag-HY Zeolite. Commercially available H-USY zeolite features the lowest framework electron density among all cation-counterbalanced Y zeolites (see Figure 1); thus it was first chosen to support Ag, in order to minimize the reduction and agglomeration of the metal. Ag-HY zeolite was prepared by cationic exchange of H-USY zeolite (Si/Al = 15) with a solution of $AgNO_3$ in water, to incorporate 1.08 wt % of Ag after calcination at 450 °C in air, according to inductively coupled plasma atomic emission spectroscopy (ICP-AES, Table S1 in the Supporting Information). This calcination temperature was chosen to decompose the nitrate ligands, as assessed by the lack of N in the elemental analysis (EA) of the calcined sample and also by the thermogravimetric analysis (TG, see Figure S8). It is worth commenting here that the cationic exchange method is preferred to the incipient wetness methodology since the former gives a homogeneous distribution of Ag cations on the zeolite surface and a stronger Ag−zeolite interaction, while the latter produces a heterogeneous distribution prone to facilitate the aggregation of Ag.

The resulting Ag^+-exchanged and calcined HY zeolite (Ag-HYcal) was characterized by powder X-ray diffraction (XRD), Brunauer−Emmett−Teller surface area analysis (BET), Fourier-transformed infrared spectroscopy (FT-IR), diffuse reflectance ultraviolet visible (DR−UV−vis) and emission spectrophotometry (fluorescence UV−vis), and X-ray photoelectron spectroscopy (XPS). In some cases, for the sake of comparison, the noncalcined Ag-HY sample (just exchanged, filtered, and dried) was also measured. The XRD analysis of the calcined sample shows that the starting diffraction peaks of the HY zeolite are preserved and that any peak corresponding to Ag nanoparticles (NPs) is not observed (Figure S1). The BET analysis gives very similar surface area and microporous volume values for both HY and Ag-HYcal solids (Figure S2), and the FT-IR spectrum also confirms the integrity of the aluminosilicate composition after the calcination (Figure S3). DR−UV−vis measurements of Ag-HY, before and after calcination, show bands between 200 and 240 nm associated with few-atom Ag^+ species,[19] and the absence of any plasmonic band of Ag NPs (400−450 nm) for Ag-HY but only the appearance of a very small band at ∼360 nm for Ag-HYcal (Figure S4) confirms the exclusive formation of subnanometric Ag entities. The corresponding fluorescence UV−vis spectra at excitation wavelengths of 200 to 260 nm, where 2−10 Ag atom clusters should emit,[20] show new fluorescence bands for the Ag-HY solid with respect to HY, at excitation wavelengths of 200−210 nm, with a Stokes shift of ∼150 nm, assignable to Ag_2 and Ag_3 clusters (Figure S5).[21] The corresponding XPS analysis suggests only the formation of Ag^+ sites on the HY zeolite, without extensive metallic Ag (Figure S6).[22] A very slight shift of the Ag $3d_{5/2}$ toward lower values can be assigned to minor Ag^0 species. Thus, the lack of Ag NP diffraction peaks, plasmonic bands, and fluorescence signals for >3 Ag atoms in the Ag-HY material, together with its high pore volume and XPS analysis, suggests that Ag is neither reduced nor severely aggregated within the HY zeolite and that all the supported Ag must be in cationic form.

In order to further check the oxidation and aggregation state of cationic Ag^+ in Ag-HY, diffuse reflectance infrared Fourier transform spectroscopy (DRIFTS) with carbon monoxide (CO) as a probe and also X-ray absorption spectroscopy (XAS) experiments, including X-ray absorption near edge structure (XANES) and extended X-ray absorption fine structure (EXAFS) measurements, were carried out. Figure 2 shows the results. The low-temperature DRIFTS-CO analysis shows main bands at 2180 and 2192 cm^{-1}, assignable to linearly coordinated $Ag^+(CO)$ and $Ag^+(CO)_2$, respectively,[6c,21] together with the expected band at 2158 cm^{-1} corresponding to the interaction between CO and the strong protons of HY zeolite.[23] Although some minor bands can be detected at lower wavenumbers (i.e., the band at 2133 cm^{-1}), it can be said here that cationic Ag species are mainly observed for the Ag-HY sample.[6c,22,24]

The XANES and EXAFS spectra, also shown in Figure 2, confirm that the Ag-HY zeolite mainly contains cationic Ag, since the spectral lines for the zeolites, either calcined or not, are more similar to Ag_2O than to Ag foil.[13b] The EXAFS spectra also support the concomitant formation of single Ag cations and very small Ag oxide clusters in Ag-HYcal, since the main peaks of the material appear at distances of ∼1.8 and 2.5 Å, attributable to Ag−O and Ag−Ag bonds, respectively.

With all the above characterization in hand, we must conclude that Ag-HYcal is constituted by ultrasmall cationic Ag entities, i.e., single cations and two to three Ag atom oxide clusters, supported in the unmodified HY zeolite framework.

2. Carbene Insertion Reactions into C−C, C−H, and O−H Bonds Catalyzed by the Ag-HY Zeolite. The new Ag-HY and Ag-HYcal zeolites were tested as catalysts for the Buchner reaction, a classical transformation in organic synthesis where a direct insertion of a carbene into the aromatic C−H bond followed by a C−C bond rearrangement occurs, which leads to otherwise very difficult to obtain cycloheptatrienes.[25] Table 1 shows the catalytic results for the reaction between ethyldiazoacetate (EDA) **1** and toluene **2** as a solvent (0.15 M), at 60 °C. For this aromatic substrate, alternatively, the insertion of the carbene into the methyl C−H bond to give the corresponding benzyl ester could also occur. The results show that the reaction does not proceed without a catalyst (entry 1), and soluble $AgNO_3$ gives an 80% yield of the products (entry 2), mainly C−H insertion. The benchmark

https://doi.org/10.1021/jacs.3c08317
J. Am. Chem. Soc. 2023, 145, 24736−24745

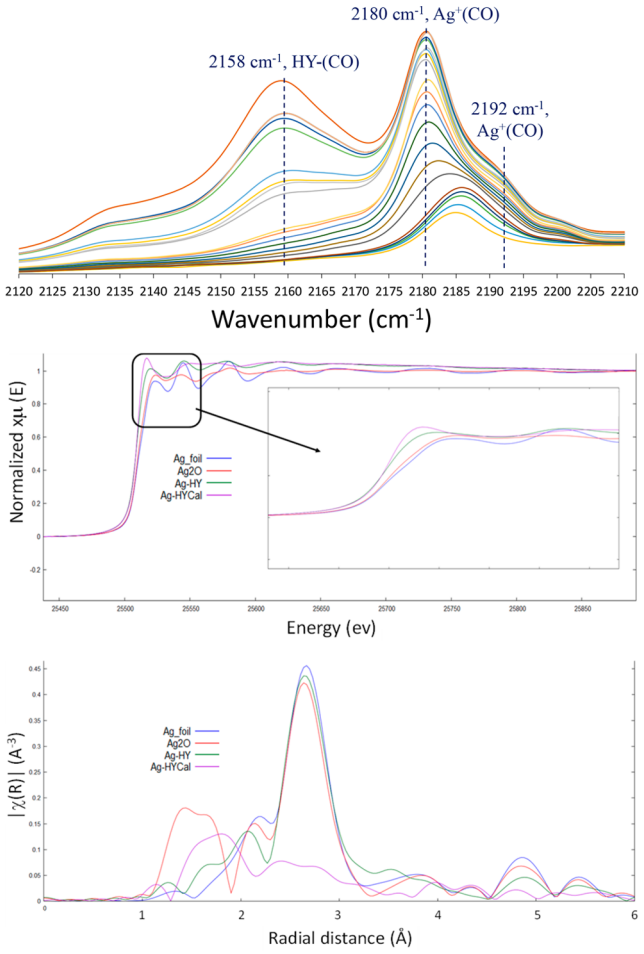

Figure 2. Top: Diffuse reflectance infrared Fourier transform spectroscopy (DRIFTS) of Ag-HYcal with carbon monoxide as a probe. Bottom: X-ray absorption near edge structure (XANES) and extended X-ray absorption fine structure (EXAFS) spectra of Ag-HY (purple line) compared with the uncalcined sample (green line) and Ag foil and Ag_2O as standards (blue and red lines, respectively).

$Rh_2(OAc)_4$ catalyst for the Buchner reaction[25b] gives a 42% yield of Buchner product **3** and 20% of C−H insertion product **4** plus dimers (35%, entry 3). Thus, it seems that $AgNO_3$ is more active and more selective that $Rh_2(OAc)_4$ under the present reaction conditions. With this in mind, it could very well occur that Ag-HY is also active in the carbene-mediated reaction. Notice that products **3** and **4** are both formed after N_2 release and carbene formation, but while product **3** comes from the cyclopropanation reaction of the triplet carbene of **1** with the C=C double bonds of toluene **2** (Buchner reaction), product **4** comes from the insertion of the singlet carbene of **1** into the C−H methyl bond of **2**. In other words, both reactions follow distinct activation mechanisms for **1**, of course directed by the electronics (and perhaps sterics) of the catalytic metal site.

The noncalcined Ag-HY zeolite shows complete conversion of **1**; however, to our surprise, the main products found were **5** and **6**, presumably coming from the insertion of the carbene in the O−H bond of water present in the zeolite (entry 4),[26] and only a 19% yield of C−H coupled products could be obtained. After calcination, Ag-HYcal shows a significant increase toward the C−C bond-forming coupled products **3** (5%) and **4** (31%); however, the main product still comes from water

Table 1. Results for the Reaction of Ethyldiazoacetate (EDA) 1 in Toluene Solvent (0.15 M) with Different Catalysts (3 mol %) under the Indicated Reaction Conditions

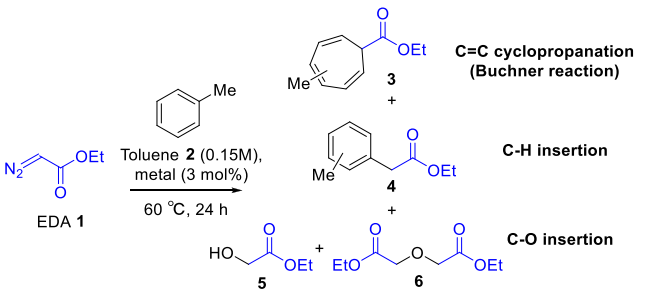

		product yield (%)		
entry	catalyst	**3**	**4**	**5 + 6**
1		3		
2	$AgNO_3$	20	60	
3[a]	$Rh_2(OAc)_4$	42	20	−
4	**Ag-HY**	**5**	**14**	77 + 4
5	Ag-HYcal	5	31	50 + 12
6	Ag-HYcal and dried	6	31	50 + 11
7	Ag-HYcal (reused)	25	33	− + 42
8	**Ag-HYcal (6th reuse)**	**47**	**38**	**− + 14**
9	$Ag-Al_2O_3$ (5 wt % Ag)	23	16	
10	Ag-hydrotalcite (5 wt % Ag)		5	
11	Ag-LiNaYcal	30	20	46 + −
12	**Ag-LiNaYcal and dried**	**55**	**42**	
13	Ag-NaYcal	14	8	48 + −
14	**Ag-NaYcal and dried**	**60**	**37**	
15	Ag-KNaYcal	15	5	50 + −
16	Ag-KNaYcal and dried	43	25	−
17	Ag-CsNaY	4	2	43 + −

[a]A 35% yield for dimers diethyl fumarate and diethyl maleate was obtained.

insertion (62%, entry 5). This result indicates that the more strongly adsorbed water molecules in the Ag-exchanged HY zeolite are acting as a reactant during the carbene reaction.

Reaction tests with 1 or 10 equiv of externally added water were carried out (Figure S7), and the results show that the reaction proceeds with complete conversion of **1** and that the product selectivity is not much varied, in other words, that external water does not participate during the O−H insertion found. Indeed, the in situ drying of the zeolite by applying vacuum at 250 °C before reaction did not improve the yield toward **3** + **4** (entry 6). Since the Ag-HYcal zeolite has lost most of the physisorbed water molecules but keeps the strongly chemisorbed water according to the corresponding TG (Figure S8), it could happen that the reuse of the zeolite will eliminate most of the O−H insertion products throughout the reuses, since chemisorbed water would become already reacted in the previous use and any external water added by the reagents would just exert a minimal influence in the reaction. In other words, the reaction of the zeolite with **1** was used as a method to deeply dry the zeolite framework of any adsorbed water molecules.

Figure 3 shows that the Ag-HYcal zeolite catalyst can be reused up to seven times without depletion in catalytic activity (>90% conversion) and much better selectivity toward the C−C bond forming products **3** and **4** (>80% in uses 5−7; see also

https://doi.org/10.1021/jacs.3c08317
J. Am. Chem. Soc. 2023, 145, 24736−24745

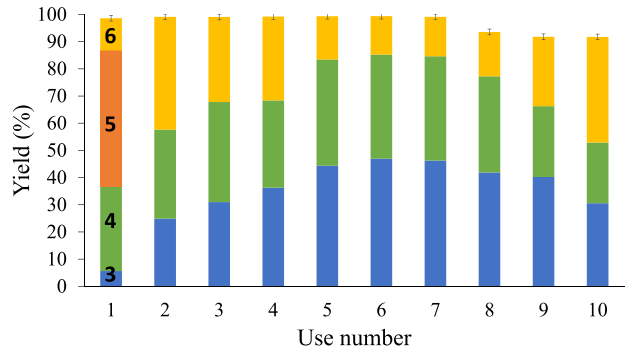

Figure 3. Reuses of Ag-HYcal as a catalyst (3 mol % Ag) for the reaction of ethyldiazoacetate (EDA) **1** in toluene solvent (0.15 M), at 60 °C for 24 h. Error bars account for a 5% uncertainty. See the structures of products **3**−**6** in Table 1. Zeolites were dried at 250 °C under vacuum overnight, when indicated.

entries 7 and 8 in Table 1) as chemisorbed water reacts. It is true that the O−H insertion products start to appear again after the eighth use, which could be due to the accumulation of water in the zeolite throughout the reuses. Notice that the removal of chemisorbed water at 400 °C under vacuum overnight resulted in the zeolite color rapidly changing to brown, a much lower conversion being found when used as a catalyst, and the only products being found were those coming from water (products **5** and **6**), reflecting that some water was still there. In other words, attempts to thermally remove the chemisorbed water in the Ag zeolite only led to a severe decomposition of the catalytically active Ag species. It is also noteworthy that the typical dimerization products for **1**, i.e., diethyl fumarate and diethyl maleate, are not observed, since the isolated supported Ag sites avoid the encountering of two carbene fragments, which is an additional advantage of the supported catalyst,[25b] while the $Rh_2(OAc)_4$ catalyst gives significant amounts of these dimers (entry 3).

Supported Ag NPs were also tested as catalysts for the reaction. For that, Ag NPs were prepared on alumina (Al_2O_3) and hydrotalcite (5 wt % Ag), with a very low NP average size of ∼2 nm according to high-resolution transmission electron microscopy (HR-TEM) images (Figure S9). Table 1 shows that these nanoparticulate Ag-supported species, even extremely small, are barely active for the reaction (entries 9 and 10), regardless of the support employed. It is very possible that subnanometric Ag species coexist with the ultrasmall Ag NPs on the Ag-Al_2O_3 and Ag-hydrotalcite solids; however, they are not active in the reaction either because of a too reduced oxidation state (Ag^0) or because of the lack of confinement effects. In any case, with this evidence in hand, we must conclude that the ultrasmall cationic Ag species present in the HY zeolite are responsible for the catalytic activity during reaction.

3. Synthesis and Characterization of Ag-(Li to Cs)NaY Zeolites and Catalytic Activity for Carbene Insertion Reactions. The change in the group I counterbalancing cation of the zeolite, from H^+ to Cs^+, leads to an increase in the electron density of the framework, which is ultimately reflected in the electronics of the supported Ag cations.[27] Thus, in principle, we can manipulate the electronics of the catalytic Ag site by simply changing the counterbalancing cation of zeolite Y.[15b] Following this rationale, we prepared the different alkaline cation-exchanged Y zeolites by standard aqueous exchange of the commercially available NaY zeolite (Si/Al = 2.5) with the corresponding acetate salt solutions, and then, Ag was incorporated by the same procedure as for Ag-HY, to obtain Ag-(Li to Cs)NaY zeolites. The alkaline cation exchange values are between 5 and 50 wt %, and the Ag content is ∼1 wt % in all cases (Table S1). Calcination at 450 °C was carried out for all zeolites except for Ag-CsNaY, since Ag is rapidly reduced even after simple drying in an oven at 100 °C (dryness was performed by prolonged vacuum).

The spontaneous reduction of Ag inside the CsNaY zeolite reflects the tendency of the supported Ag cations to accept electrons from the zeolite framework, particularly from the CsNaY zeolite.[28] In accordance with this, a comparative XRD analysis of the different Ag-Y zeolites shows the progressive appearance of the (111), (200), (220), and (311) crystallographic planes of Ag NPs as the zeolite framework gets more electron rich, from H^+ to Cs^+ (Figure S1).[29,30] In any case, the aluminosilicate zeolitic structure remains stable, as assessed by FT-IR (Figure S3). The Ag-$3d_{5/2}$ XPS signals show a very slight shift toward higher electron-binding values (Figure S6) when going from HY to CsNaY, and this shift toward higher electron-binding values is also reflected in the corresponding Si 2p (Figure S10), Al 2p (Figure S11), and O 1s (Figure S12) XPS signals.[31] These results, together, strongly support the transference and modification of the electron density on the Ag site in the different metal-supported zeolites.

The new Ag-zeolites were tested for the reaction between EDA **1** and toluene **2**. Table 1 shows that the calcined cation-exchanged zeolite samples behave as Ag-HYcal, to give similar catalytic results (compare entries 5, 11, 13, and 15), and the corresponding kinetic results confirmed that the Ag-HYcal catalyst is the more active among them under these reaction conditions (Figure S13). However, if the Ag-zeolite catalyst is dried in situ before adding the reactants, the O−H insertion products **5** and **6** disappear and only the C−C coupling products **3** and **4** are formed, in yields of up to 97% with Ag-LiNaY and Ag-NaY (Table 1, entries 12 and 14, respectively). A hot filtration test for Ag-LiNaY shows that there is not any catalytically active species in solution (Figure S14), confirming the heterogeneous nature of the catalysis and the stability of the zeolite in reaction. In accordance, the XRD and FT-IR spectra of the used Ag-LiNaY catalyst are similar to those of the fresh zeolite sample (Figures S15 and S16, respectively). Ag-CsNaY, which shows the highest amount of Ag^0 species and cannot be dried at >100 °C prior to reaction, gives poor catalytic results (Table 1, entry 17).

The higher catalytic activity of the alkaline-exchanged zeolites with respect to Ag-HY toward the C−C bond-forming products **3** and **4** could be due to an intrinsic higher selectivity of the Ag catalytic site for C−C and C−H bond activation or simply to a lack of water in the zeolite once dried. However, the FT-IR spectra of the calcined solids show similar amounts of adsorbed water in all zeolites (Figure S3). In order to check if Ag-(Li to K)NaYcal zeolites are less catalytically active than Ag-HYcal toward the insertion of the carbene in the O−H bonds, the catalytic reaction of EDA **1** in a mixture of water/ethanol **7** was performed. Ethanol **7** was coadded to water in order to assess the reactivity of an external O−H bond, not present in the zeolite. The results in Figure 4 show that the Ag-HYcal catalyst gives three times more yield of O−H insertion products **5** + **8** than the alkaline zeolites; indeed, product **8** is the major product. Thus, we can conclude that the higher catalytic activity of Ag-(Li to K)NaYcal zeolites to products **3**

https://doi.org/10.1021/jacs.3c08317
J. Am. Chem. Soc. 2023, 145, 24736−24745

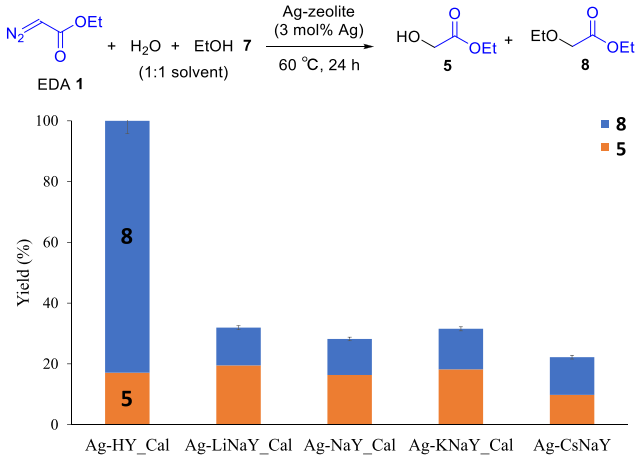

Figure 4. Catalytic results for the reaction of ethyldiazoacetate (EDA) **1** in a 1:1 v/v mixture of water/ethanol (0.15 M) with different Ag-zeolites as catalysts (3 mol % Ag), at 60 °C for 24 h. Zeolites were dried at 250 °C under vacuum overnight except for Ag-CsNaY. Error bars account for a 5% uncertainty.

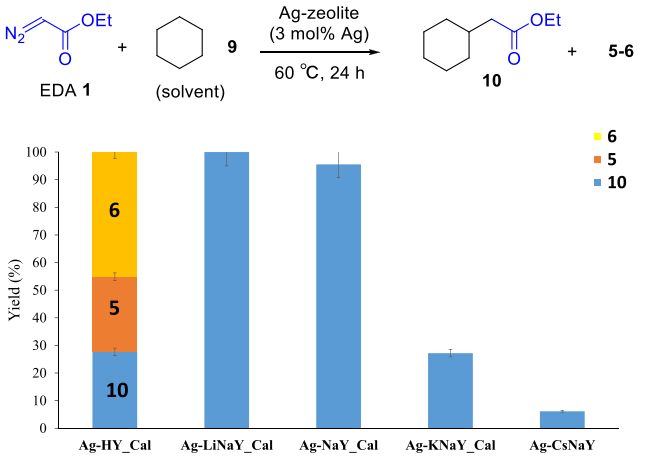

Figure 5. Catalytic results for the reaction of ethyldiazoacetate (EDA) **1** in cyclohexane **9** (0.15 M) with different Ag-zeolites as catalysts (3 mol % Ag), at 60 °C for 24 h. Zeolites were dried at 250 °C under vacuum overnight, except for Ag-CsNaY. Error bars account for a 5% uncertainty.

and **4** comes from a better intrinsic selectivity of the Ag catalysts toward C−C and C−H bond activation, while Ag-HYcal prefers to activate and insert the carbene in O−H bonds. Indeed, other alcohols such as 2-chloroethanol (98% yield), phenylethanol (98% yield), allyl alcohol (97% yield), and propargyl alcohol (95% yield) engaged extremely well in the Ag-HYcal-catalyzed reaction. In summary, the counter cation nature and not the water content is the major parameter affecting the activity and selectivity of the carbene insertion reaction: while HY directs the insertion toward O−H bonds in the presence of O-containing nucleophiles (such as water and alcohols) and toward C−C and C−H bonds, equally, without water in the reaction media, alkaline-earth cations divert the insertion toward C−C and C−H bonds, in an approximately 1:2 ratio (Figure S17). These selectivity results make sense if we consider that O−H bonds are much more polar than C═C or C−H bonds; thus, the higher the electron deficiency in the Ag catalytic site (the more Lewis acid the Ag is), the better the activation of the O−H vs C═C or C−H bonds.

The high catalytic activity of the Ag-(Li to Cs)NaYcal zeolites to C−H insertion reactions opens the door for more challenging transformations, such as the insertion of EDA **1** in neat alkanes. Figure 5 shows that cyclohexane **9** incorporates the carbene from **1** in >95% yield with complete selectivity to product **10** on either the Ag-LiNaYcal or Ag-NaYcal catalyst. Such an excellent product yield for **10** is rarely found for any solid catalyst as far as we know.

4. Nature of the Catalytically Active Ag Species on Ag-LiNaY Zeolite and Detection of the Solid-Supported Ag-Carbene Species. Aberration-corrected high-angle annular dark-field scanning transmission electron microscopy (AC HAADF-STEM) measurements of a Ag-LiNaYcal sample were carried out, and they are shown in Figure 6 (top). The energy-dispersive X-ray spectroscopy (EDX) mapping of a zeolite crystallite confirms the homogeneous distribution of all elements in the zeolite, including Ag (see also Figure S18), which shows a minor degree of aggregation in the form of NPs, in accordance with the XRD analysis (see Figure S1). Elemental EDX quantification fits well with the ICP-AES results (Table S1).

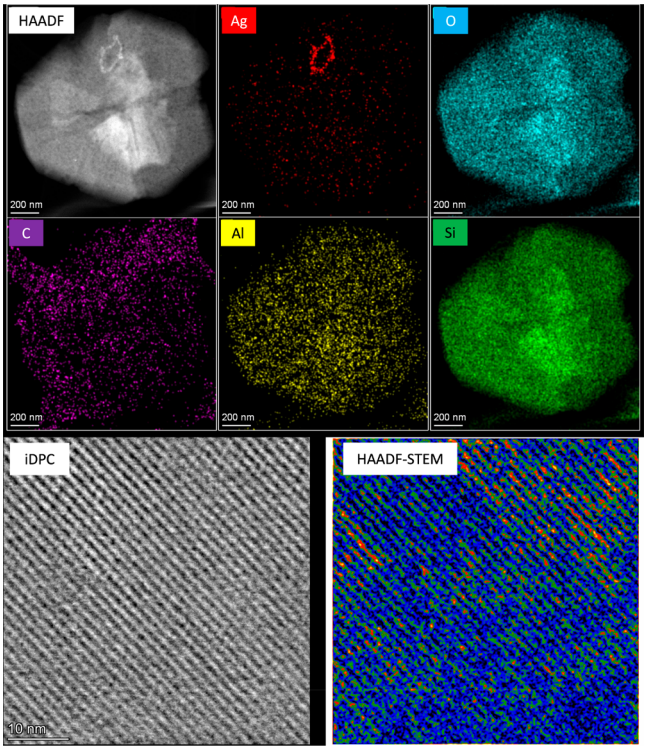

Figure 6. Top: Compositional mapping of a representative AC HAADF-STEM image of a Ag-LiNaYcal crystallite using EDX spectroscopy to detect the different elements. Bottom: High-resolution AC HAADF-STEM (left) and iDPC (right) images of a Ag-LiNaYcal sample. The identification of Ag entities is performed on the HAADF image due to the higher contrast and by means of iDPC images, to reveal the atomic structure of the zeolite LiNaYcal (see also Figure S19). The identification and location of the subnanometric (<1 nm) Ag entities within the zeolite framework are obtained by combining the images obtained in these two modes.

Figure 6 (bottom) shows aberration-corrected scanning transmission electron microscopy (AC-STEM) images of the Ag-LiNaYcal sample at 2 million times magnification. The integrated differential phase contrast (iDPC) image shows low-*Z* elements with bright contrast and dark background. The

https://doi.org/10.1021/jacs.3c08317
J. Am. Chem. Soc. 2023, 145, 24736−24745

colored HAADF-STEM image can reliably identify Ag species as the brightest contrasts in these images, since HAADF-STEM imaging is proportional in good approximation to the squared atomic number, Z^2. Furthermore, the visualization of the Ag entities has been improved by submitting raw HAADF images to advanced image processing, which included denoising and background subtraction (see Figure S20). In order to determine in a fully automated, user-independent, and statistically meaningful way the size of the Ag clusters observed in the experimental images, a segmentation based on K-means clustering techniques was performed on the HAADF-STEM images.[15b,32] The application of the K-means clustering method to the experimental images reveals the major presence of Ag single atoms and ultrasmall clusters together with minor Ag NPs detected (see also Figure S21). Modeling and image simulations (Figures S22 and S23) confirm these results. All these results, together, noticeably evidence that the majority of Ag species inside the zeolite corresponds to Ag single atoms and ultrasmall Ag clusters, in good accordance with the DR−UV−vis, DRIFTS, and XAS results shown above for the Ag-HY zeolite.

Figure 7 shows the ^{13}C cross-polarization magic angle-spinning nuclear magnetic resonance (^{13}C CP/MAS NMR)

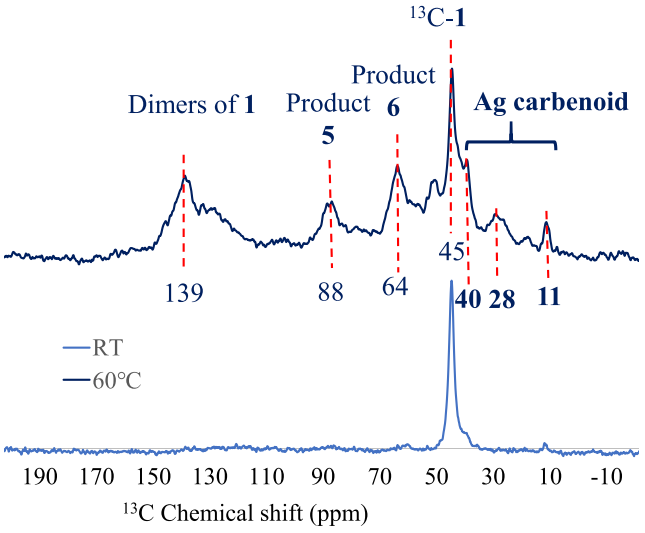

Figure 7. ^{13}C cross-polarization magic angle-spinning nuclear magnetic resonance (^{13}C CP/MAS NMR) spectra of **1**-^{13}C[12a] and after reaction of EDA **1** within the Ag-LiNaYcal zeolite.

spectrum of adsorbed, isotopically labeled EtOOC^{13}CHN$_2$ (^{13}C-**1**)[33] and the resulting spectrum after sealing an ampule with EDA **1** and an equimolecular amount of Ag in Ag-LiNaYcal zeolite and making them react at 60 °C for 3 days. The CP NMR technique visualizes the carbon atoms containing C−H bonds and, thus, in our case, the carbene atom in **1**. It can be seen that the original signal of **1** at 45 ppm disappears in the presence of stoichiometric Ag, to give new upshielded signals at 11, 28, and 40 ppm, compatible with a metal carbenoid coordinated through the sp^2 O atom of the carbonyl group to the Ag species (see Figure 9).[18a,34] Besides, the signals corresponding to the expected products with the water molecules in the zeolite at 64 ppm (product **6**) and 88 ppm (product **5**) are also observed, as well as some dimers produced under these stoichiometric reaction conditions (139

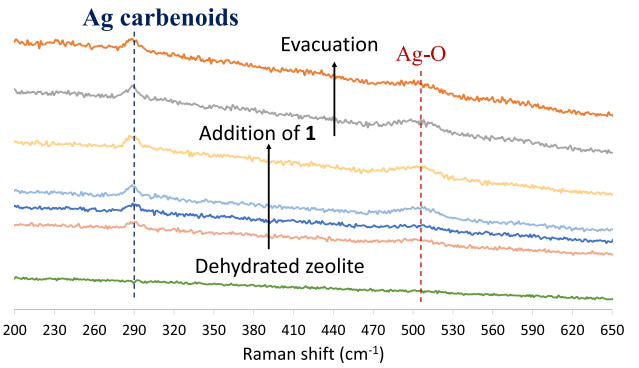

Figure 8. Raman spectroscopy of the Ag-LiNaY zeolite after dosing EDA **1** (four shots) and evacuation under vacuum (twice).

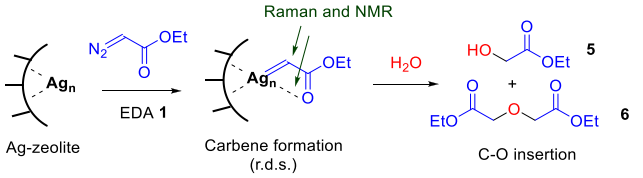

Figure 9. Proposed reaction mechanism for the carbene formation and water insertion on the Ag-zeolite catalyst (rds: rate-determining step), also showing the possible configuration of the Ag carbene intermediate according to the Raman and ^{13}C CP/MAS NMR spectra.[18a,34]

ppm). Notice that the ester signals at ∼170 ppm are not detected because they do not contain CH bonds.

Figure 8 shows the corresponding time-resolved Raman spectra of the Ag-LiNaY zeolite after dosing EDA **1**, and new bands at ∼290 and 510 cm^{-1} appear, which correspond to reported metal carbene complexes[18a] and Ag−O bonds,[18a,21] respectively, with the sp^2 ester O atom coordination. These bands are stable and remain after vacuum evacuation of the sample.

In order to have more information about the reaction pathway and give the reaction mode at a molecular level, we performed kinetic analysis with increasing amounts of the different reagents (semistationary state conditions) to calculate the reaction order for each reagent and, thus, the rate equation. The results (Figure S24) show a reaction order for the Ag-HYcal zeolite catalyst, EDA **1**, and water of 1, 1, and 0, respectively. The same result for EDA **1** is found with the Ag-LiNaYcal zeolite catalyst. Therefore, the rate equation can be written as $v_0 = k_{exp}$[Ag-zeolite][EDA **1**], indicating that the rate-determining step (rds) of the reaction involves the formation of the Ag-carbene complex. This is the reason that the carbene intermediate is just briefly seen since, after being formed, it rapidly reacts with water to give products **5** and **6**.

With all this information in hand, the proposed mechanism for the reaction with water is shown in Figure 9, which also includes the configuration of the carbene Ag-zeolite. The first step of the process is the formation of the Ag carbene, which is the rds of the reaction. The configuration of this carbene intermediate shows that the carbonyl ester group coordinates to the metal site, as informed by the Raman and ^{13}C CP/MAS NMR spectra.[18a,34] This carbene is then inserted into the O−H bond of water to give the final product **5** (and then **6** by subsequent carbene insertion) and regenerate the starting Ag-zeolite catalyst.

https://doi.org/10.1021/jacs.3c08317
J. Am. Chem. Soc. 2023, 145, 24736−24745

During the reaction order studies for the Ag-HYcal zeolite catalyst, we found that the amount of Ag-zeolite can be decreased very significantly, to ≤0.1 mol % in Ag, to obtain significant conversion after just 30 min of reaction. In this way, a much better selectivity for the C−C and C−H insertion products is obtained since the amount of water provided by the zeolite is minimized. Figure 10 shows this new result, which indicates that the catalytic activity of Ag in the zeolite is remarkable.

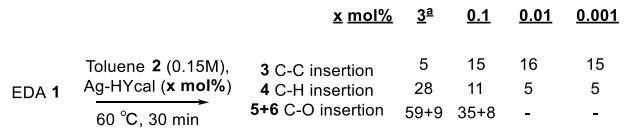

Figure 10. Reaction results for decreasing amounts of Ag-HYcal zeolite catalyst after 30 min of reaction time. [a] Results for 24 h of reaction time.

The combined HR HAADF-STEM, ^{13}C CP/MAS NMR, and Raman results strongly support that Ag_n-carbene complexes are formed within the zeolite, where n = 1−3. The selectivity toward one or another product depends on the Ag electronics, modulated by the zeolite, in such a way that electron-poor zeolites such as HY stabilize highly cationic Ag species to catalyze the insertion of the carbene in O−H bonds, while Li- to K-exchanged zeolites stabilize less cationic Ag species to catalyze the insertion of the carbene in C−H bonds. However, the stability of Ag species in less acidic zeolites seems to be lower according to reusability tests with Ag-LiNaYcal zeolite (Figure S25) and TEM analysis (Figure S26, Ag nanoparticles can be seen). Despite many reactions being investigated, these reactions can be classified in basically two groups—C−H and O−H carbene insertions—and the selectivity for one or another is the main activity of the zeolite catalysts studied here.

CONCLUSIONS

The synthesis of ultrasmall Ag species in zeolite Y has been achieved by a simple exchange−calcination procedure to obtain cationic single- and few-atom silver clusters. This supported Ag zeolites catalyze carbene-mediated organic reactions with high yield and selectivity, including cyclohexane as a substrate, depending on the zeolite counterbalancing cation, which dictates the electronics of the Ag active site. The amount of catalyst in the reaction can be as low as ≤0.1 mol % Ag. These results showcase the high catalytic activity of Ag in organic synthesis when obtained in subnanometric form[35] and the use of zeolites as easily tunable macroligands to generate and stabilize such ultrasmall supported metal species.[36] Incidentally, we have found a method to deeply dry the HY zeolite by making the strongly adsorbed water react with the in situ formed carbenes.

ASSOCIATED CONTENT

Supporting Information

The Supporting Information is available free of charge at https://pubs.acs.org/doi/10.1021/jacs.3c08317.

Experimental section, including the synthesis of the materials and the reaction procedures, and Supporting Table S1 and Figures S1−S26 (PDF)

AUTHOR INFORMATION

Corresponding Authors

Marta Mon − *Instituto de Tecnología Química (UPV-CSIC), Universitat Politècnica de València−Consejo Superior de Investigaciones Científicas, 46022 Valencia, Spain*; Email: marmoco@upv.itq.es

Antonio Leyva-Pérez − *Instituto de Tecnología Química (UPV-CSIC), Universitat Politècnica de València−Consejo Superior de Investigaciones Científicas, 46022 Valencia, Spain*; orcid.org/0000-0003-1063-5811; Email: anleyva@upv.itq.es

Authors

Yongkun Zheng − *Instituto de Tecnología Química (UPV-CSIC), Universitat Politècnica de València−Consejo Superior de Investigaciones Científicas, 46022 Valencia, Spain*

Alejandro Vidal-Moya − *Instituto de Tecnología Química (UPV-CSIC), Universitat Politècnica de València−Consejo Superior de Investigaciones Científicas, 46022 Valencia, Spain*

Juan Carlos Hernández-Garrido − *Departamento de Ciencia de los Materiales e Ingeniería Metalúrgica y Química Inorgánica, Facultad de Ciencias, Universidad de Cádiz, 11510 Puerto Real, Cádiz, Spain*; orcid.org/0000-0001-8499-0395

Complete contact information is available at: https://pubs.acs.org/10.1021/jacs.3c08317

Author Contributions

All authors have participated in the writing of the manuscript and have approved the final version.

Notes

The authors declare no competing financial interest.

ACKNOWLEDGMENTS

This work is part of the project PID2020-115100GB-I00 funded by MCIN/AEI/10.13039/501100011033MICIIN (Spain). Thanks are extended to the TED2021-130465B-I00 project of the MICIIN. Financial support by the Severo Ochoa Centre of Excellence Program (CEX2021-001230-S) is gratefully acknowledged. M.M. thanks MICIIN for a contract under the Juan de la Cierva program (FJC2019-040523-I). Y.Z. thanks the China Scholarship Council (CSC No. 202009350009) for a Ph.D. fellowship. The AC-STEM data were obtained at the DME-UCA node of the Spanish Unique Scientific and Technological Infrastructure (ICTS) of Electron Microscopy of Materials, ELECMIM.

REFERENCES

(1) Sun, T.; Seff, K. Silver Clusters and Chemistry in Zeolites. *Chem. Rev.* **1994**, *94* (4), 857−870.

(2) (a) Boschetto, D. L.; Lerin, L.; Cansian, R.; Pergher, S. B. C.; Di Luccio, M. Preparation and Antimicrobial Activity of Polyethylene Composite Films with Silver Exchanged Zeolite−Y. *Chem. Eng. J.* **2012**, *204*, 210−216. (b) Singh, V. V.; Jurado-Sánchez, B.; Sattayasamitsathit, S.; Orozco, J.; Li, J.; Galarnyk, M.; Fedorak, Y.; Wang, J. Multifunctional Silver−Exchanged Zeolite Micromotors for Catalytic Detoxification of Chemical and Biological Threats. *Adv. Funct. Mater.* **2015**, *25* (14), 2147−2155. (c) Cerrillo, J. L.; Palomares, A. E.; Rey, F.; Valencia, S.; Palou, L.; Pérez-Gago, M. B. Ag−Zeolites as Fungicidal Material: Control of Citrus Green Mold Caused by Penicillium Digitatum. *Microporous Mesoporous Mater.* **2017**, *254*, 69−76. (d) Cerrillo, J.; Palomares, A.; Rey, F. Silver Exchanged Zeolites as Bactericidal Additives in Polymeric Materials. *Microporous Mesoporous Mater.* **2020**, *305*, 110367.

(3) Chebbi, M.; Azambre, B.; Cantrel, L.; Huvé, M.; Albiol, T. Influence of Structural, Textural and Chemical Parameters of Silver Zeolites on the Retention of Methyl Iodide. *Microporous Mesoporous Mater.* **2017**, *244*, 137−150. (b) Azambre, B.; Chebbi, M. Evaluation of Silver Zeolites Sorbents toward Their Ability to Promote Stable CH_3I Storage as AgI Precipitates. *ACS Appl. Mater. Interfaces* **2017**, *9* (30), 25194−25203.

(4) (a) Shi, C.; Cheng, M.; Qu, Z.; Bao, X. Investigation on the Catalytic Roles of Silver Species in the Selective Catalytic Reduction of NO_x with Methane. *Appl. Catal. B: Environ.* **2004**, *51* (3), 171−181. (b) Baba, T. Conversion of Methane over Ag^+−exchanged Zeolite in the Presence of Ethene. *Catal. Surv. Asia* **2005**, *9*, 147−154. (c) Baba, T.; Iwase, Y.; Inazu, K.; Masih, D.; Matsumoto, A. Catalytic Properties of Silver−Exchanged Zeolites for Propene Production by Conversion of Methane in the Presence of Ethene. *Microporous Mesoporous Mater.* **2007**, *101* (1−2), 142−147.

(5) Sugihara, H.; Chen, L. Y.; Yasumori, I. The Catalytic Activity of AgX−Type Zeolite for the Isomerization of 1−Butene. *Bull. Chem. Soc. Jpn.* **1974**, *47* (9), 2089−2093.

(6) (a) Teng, J. W.; Cai, T. X.; Bao, X. H. Ag-ZSM-5 Catalyst for the Catalytic Decomposition of NO. *Chin. Chem. Lett.* **1999**, *10* (1), 83−86. (b) Lagunov, O.; Chakarova, K.; Hadjiivanov, K. Silver−Catalyzed Low−Temperature CO Isotopic Scrambling Reaction: $^{12}C^{16}O+ {}^{13}C^{18}O \rightarrow {}^{12}C^{18}O+ {}^{13}C^{16}O$. *Phys. Chem. Chem. Phys.* **2012**, *14* (7), 2178−2182. (c) Tarach, K.; Góra-Marek, K.; Chrzan, M.; Walas, S. Quantification of Silver Sites in Zeolites: Carbon Monoxide Sorption Monitored by IR Spectroscopy. *J. Phys. Chem. C* **2014**, *118* (41), 23751−23760. (d) Martinez-Ortigosa, J.; Lopes, C. W.; Agostini, G.; Palomares, A. E.; Blasco, T.; Rey, F. AgY Zeolite as Catalyst for the Selective Catalytic Oxidation of NH_3. *Microporous Mesoporous Mater.* **2021**, *323*, 111230.

(7) (a) Beer, R.; Binder, F.; Calzaferri, G. Photochemical Oxidation of Water on a 1 M Ag^+ Zeolite Layer. *J. Photochem. Photobiol., A* **1992**, *69* (1), 67−72. (b) Kennes, K.; Coutino-Gonzalez, E.; Martin, C.; Baekelant, W.; Roeffaers, M. B.; Van der Auweraer, M. Silver Zeolite Composites-Based Leds: A Novel Solid-State Lighting Approach. *Adv. Funct. Mater.* **2017**, *27* (14), 1606411. (c) Baekelant, W.; Aghakhani, S.; Coutino-Gonzalez, E.; Kennes, K.; D'Acapito, F.; Grandjean, D.; Van der Auweraer, M.; Lievens, P.; Roeffaers, M. B. J.; Hofkens, J.; Steele, J. A. Shaping the Optical Properties of Silver Clusters inside Zeolite a Via Guest−Host−Guest Interactions. *J. Phys. Chem. Lett.* **2018**, *9* (18), 5344−5350. (d) Lopes, C. W.; Martinez-Ortigosa, J.; Góra-Marek, K.; Tarach, K.; Vidal-Moya, J. A.; Palomares, A. E.; Agostini, G.; Blasco, T.; Rey, F. Zeolite−Driven Ag Species During Redox Treatments and Catalytic Implications for SCO of NH_3. *J. Mater. Chem. A* **2021**, *9* (48), 27448−27458. (e) Li, N.; Huang, B.; Dong, X.; Luo, J.; Wang, Y.; Wang, H.; Miao, D.; Pan, Y.; Jiao, F.; Xiao, J. Bifunctional Zeolites−Silver Catalyst Enabled Tandem Oxidation of Formaldehyde at Low Temperatures. *Nat. Commun.* **2022**, *13* (1), 2209.

(8) For reviews see: (a) Li, M.; Wu, W.; Jiang, H. Recent Advances in Silver-Catalyzed Transformations of Electronically Unbiased Alkenes and Alkynes. *ChemCatChem.* **2020**, *12* (20), 5034−5050. (b) Sekine, K.; Yamada, T. Silver−Catalyzed Carboxylation. *Chem. Soc. Rev.* **2016**, *45* (16), 4524−4532. (c) Fang, G.; Bi, X. Silver−Catalysed Reactions of Alkynes: Recent Advances. *Chem. Soc. Rev.* **2015**, *44* (22), 8124−8173. (d) Naodovic, M.; Yamamoto, H. Asymmetric Silver−Catalyzed Reactions. *Chem. Rev.* **2008**, *108* (8), 3132−3148. (e) Thompson, J. L.; Davies, H. M. Enhancement of Cyclopropanation Chemistry in the Silver−Catalyzed Reactions of Aryldiazoacetates. *J. Am. Chem. Soc.* **2007**, *129* (19), 6090−6091. For a book Chapter see (f) Hashmi, A. S. K. A Critical Comparison: Copper, Silver and Gold. In *Silver in Organic Chemistry*; Harmata, M., Ed.; John Wiley and Sons, Inc.: Hoboken, 2010; Chapter 12, pp 357−379.

(9) For representative articles see: (a) Fructos, M. R.; Belderrain, T. R.; de Frémont, P.; Scott, N. M.; Nolan, S. P.; Díaz-Requejo, M. M.; Pérez, P. J. A Gold Catalyst for Carbene−Transfer Reactions from Ethyl Diazoacetate. *Angew. Chem., Int. Ed.* **2005**, *44* (33), 5284−5288. (b) Caballero, A.; Despagnet-Ayoub, E.; Mar Díaz-Requejo, M.; Díaz-Rodríguez, A.; González-Núñez, M. E.; Mello, R.; Muñoz, B. K.; Ojo, W.-S.; Asensio, G.; Etienne, M.; Pérez, P. J. Silver−Catalyzed C−C Bond Formation Between Methane and Ethyl Diazoacetate in Supercritical CO_2. *Science* **2011**, *332* (6031), 835−838. (c) Sanchez-Sanchez, C.; Orozco, N.; Holgado, J. P.; Beaumont, S. K.; Kyriakou, G.; Watson, D. J.; Gonzalez-Elipe, A. R.; Feria, L.; Fernandez Sanz, J.; Lambert, R. M. Sonogashira Cross−Coupling and Homocoupling on a Silver Surface: Chlorobenzene and Phenylacetylene on Ag(100). *J. Am. Chem. Soc.* **2015**, *137* (2), 940−947. (d) Clarke, A. K.; James, M. J.; O'Brien, P.; Taylor, R. J. K.; Unsworth, W. P. Silica−Supported Silver Nitrate as a Highly Active Dearomatizing Spirocyclization Catalyst: Synergistic Alkyne Activation by Silver Nanoparticles and Silica. *Angew. Chem., Int. Ed.* **2016**, *55* (44), 13798−13802. (e) Gui, Q.; Han, K.; Liu, Z.; Su, Z.; He, X.; Jiang, H.; Tian, B.; Li, Y. E−Selective Synthesis of Vinyl Sulfones Via Silver−Catalyzed Sulfonylation of Styrenes. *Org. Biomol. Chem.* **2018**, *16* (32), 5748−5751. See also the following key references from industrial research, aiming at bulk-scale transformations: (f) Dabral, S.; Bayarmagnai, B.; Hermsen, M.; Schießl, J.; Mormul, V.; Hashmi, A. S. K.; Schaub, T. Silver−catalyzed Carboxylative Cyclization of Primary Propargyl Alcohol with CO2. *Org. Lett.* **2019**, *21* (5), 1422−1425. (g) Dabral, S.; Licht, U.; Rudolf, P.; Bollmann, G.; Hashmi, A. S. K.; Schaub, T. Synthesis and polymerisation of alpha−alkylidene cyclic carbonates obtained from carbon dioxide, epoxides and the primary propargylic alcohol 1,4−butynediol. *Green Chem.* **2020**, *22* (5), 1553−1558. (h) Johnson, C.; Dabral, S.; Rudolf, P.; Licht, U.; Hashmi, A. S. K.; Schaub, T. Liquid−liquid−phase synthesis of exo−vinylene carbonates from primary propargylic alcohols: catalyst design and recycling. *ChemCatChem.* **2021**, *13* (1), 353−361.

(10) (a) Baldansuren, A.; Dilger, H.; Eichel, R. d.-A.; van Bokhoven, J. A.; Roduner, E. Interaction and Reaction of Ethylene and Oxygen on Six−Atom Silver Clusters Supported on LTA Zeolite. *J. Phys. Chem. C* **2009**, *113* (45), 19623−19632. (b) Ono, Y.; Baba, T. Unique Properties of Silver Cations in Solid−Acid Catalysis by Zeolites and Heteropolyacids. *Phys. Chem. Chem. Phys.* **2015**, *17* (24), 15637−15654.

(11) (a) Zhang, L.; Ren, Y.; Liu, W.; Wang, A.; Zhang, T. Single−Atom Catalyst: A Rising Star for Green Synthesis of Fine Chemicals. *Natl. Sci. Rev.* **2018**, *5* (5), 653−672. (b) Yan, H.; Su, C.; He, J.; Chen, W. Single−Atom Catalysts and Their Applications in Organic Chemistry. *J. Mater. Chem. A* **2018**, *6* (19), 8793−8814. (c) Hu, Y.; Li, H.; Li, Z.; Li, B.; Wang, S.; Yao, Y.; Yu, C. Progress in Batch Preparation of Single−Atom Catalysts and Application in Sustainable Synthesis of Fine Chemicals. *Green Chem.* **2021**, *23* (22), 8754−8794. (d) Li, W.-H.; Yang, J.; Wang, D.; Li, Y. Striding the Threshold of an Atom Era of Organic Synthesis by Single−Atom Catalysis. *Chem.* **2022**, *8* (1), 119−140. (e) Greco, R.; Mon, M.; Leyva-Pérez, A. Supported Metal Single Atom Thermocatalysts for C−C, C−Si, and C−B Bond−Forming (Coupling) Reactions and Biomedical Applications. In *Supported Metal Single Atom Catalysis*; Serp, P.; Minh, D. P, Eds.; John Wiley & Sons, 2022; pp 473−502. (f) Oliver-Meseguer, J.; Leyva-Pérez, A. Single atom and metal cluster catalysts in organic reactions: from the solvent to the solid. *ChemCatChem.* **2023**, *15*, e202201681.

(12) (a) Lei, Y.; Mehmood, F.; Lee, S.; Greeley, J.; Lee, B.; Seifert, S.; Winans, R. E.; Elam, J. W.; Meyer, R. J.; Redfern, P. C.; et al. Increased Silver Activity for Direct Propylene Epoxidation Via Subnanometer Size Effects. *Science* **2010**, *328* (5975), 224−228. (b) Buceta, D.; Busto, N.; Barone, G.; Leal, J. M.; Domínguez, F.; Giovanetti, L. J.; Requejo, F. G.; García, B.; López-Quintela, M. A. Ag_2 and Ag_3 Clusters: Synthesis, Characterization, and Interaction with DNA. *Angew. Chem., Int. Ed.* **2015**, *54* (26), 7612−7616. (c) Vajda, S.; White, M. G. Catalysis Applications of Size−Selected Cluster Deposition. *ACS Catal.* **2015**, *5* (12), 7152−7176.

(13) (a) Tiburcio, E.; Zheng, Y.; Mon, M.; Martín, N.; Ferrando-Soria, J.; Armentano, D.; Leyva-Pérez, A.; Pardo, E. Highly Efficient MOF−Driven Silver Subnanometer Clusters for the Catalytic Buchner Ring Expansion Reaction. *Inorg. Chem.* **2022**, *61* (30),

https://doi.org/10.1021/jacs.3c08317
J. Am. Chem. Soc. 2023, 145, 24736−24745

11796−11802. (b) Tiburcio, E.; Zheng, Y.; Bilanin, C.; Hernandez-Garrido, J. C.; Vidal-Moya, A.; Oliver-Meseguer, J.; Martin, N.; Mon, M.; Ferrando-Soria, J.; Armentano, D.; Leyva-Perez, A.; Pardo, E. MOF-Triggered Synthesis of Subnanometer Ag^0_2 Clusters and Fe^{3+} Single Atoms: Heterogenization Led to Efficient and Synergetic One-Pot Catalytic Reactions. *J. Am. Chem. Soc.* **2023**, *145*, 10342. (c) Zheng, Y.; Martín, N.; Boronat, M.; Ferrando-Soria, J.; Mon, M.; Armentano, D.; Pardo, E.; Leyva-Pérez, A. Ag2(0) Dimers Within a Thioether-Functionalized MOF Catalyze the CO2 to CH4 Hydrogenation Reaction. *Sc. Rep.* **2023**, *13*, 10376.

(14) Frising, T.; Leflaive, P. Extraframework Cation Distributions in X and Y Faujasite Zeolites: A Review. *Microporous Mesoporous Mater.* **2008**, *114* (1−3), 27−63.

(15) (a) Rubio-Marques, P.; Rivero-Crespo, M. A.; Leyva-Perez, A.; Corma, A. Well−Defined Noble Metal Single Sites in Zeolites as an Alternative to Catalysis by Insoluble Metal Salts. *J. Am. Chem. Soc.* **2015**, *137* (36), 11832−11837. (b) Garnes-Portolés, F.; Greco, R.; Oliver-Meseguer, J.; Castellanos-Soriano, J.; Consuelo Jiménez, M.; López-Haro, M.; Hernández-Garrido, J. C.; Boronat, M.; Pérez-Ruiz, R.; Leyva-Pérez, A. Regioirregular and Catalytic Mizoroki−Heck Reactions. *Nat. Catal.* **2021**, *4* (4), 293−303.

(16) For reviews see: (a) Díaz-Requejo, M. M.; Pérez, P. J. Copper, Silver and Gold−Based Catalysts for Carbene Addition or Insertion Reactions. *J. Organomet. Chem.* **2005**, *690* (24−25), 5441−5450. (b) Alderson, J. M.; Corbin, J. R.; Schomaker, J. M. Tunable, Chemo−and Site−Selective Nitrene Transfer Reactions through the Rational Design of Silver (I) Catalysts. *Acc. Chem. Res.* **2017**, *50* (9), 2147−2158.

(17) For representative recent articles see: (a) Bergstrom, B. D.; Nickerson, L. A.; Shaw, J. T.; Souza, L. W. Transition Metal Catalyzed Insertion Reactions with Donor/Donor Carbenes. *Angew. Chem., Int. Ed.* **2021**, *60* (13), 6864−6878. (b) Li, M.-L.; Pan, J.-B.; Zhou, Q.-L. Enantioselective Synthesis of Amino Acids from Ammonia. *Nat. Catal.* **2022**, *5* (6), 571−577. (c) Liu, W.; Choi, I.; Zerull, E. E.; Schomaker, J. M. Tunable Silver−Catalyzed Nitrene Transfer: From Chemoselectivity to Enantioselective C−H Amination. *ACS Catal.* **2022**, *12* (9), 5527−5539.

(18) (a) Oliver-Meseguer, J.; Boronat, M.; Vidal-Moya, A.; Concepción, P.; Rivero-Crespo, M. A.; Leyva-Pérez, A.; Corma, A. Generation and Reactivity of Electron−Rich Carbenes on the Surface of Catalytic Gold Nanoparticles. *J. Am. Chem. Soc.* **2018**, *140* (9), 3215−3218. (b) Crowley, D. C.; Brouder, T. A.; Kearney, A. M.; Lynch, D.; Ford, A.; Collins, S. G.; Maguire, A. R. Exploiting Continuous Processing for Challenging Diazo Transfer and Telescoped Copper−Catalyzed Asymmetric Transformations. *J. Org. Chem.* **2021**, *86* (20), 13955−13982.

(19) (a) Bartolomeu, R.; Bertolo, R.; Casale, S.; Fernandes, A.; Henriques, C.; da Costa, P.; Ribeiro, F. Particular Characteristics of Silver Species on Ag−Exchanged LTL Zeolite in K and H Form. *Microporous Mesoporous Mater.* **2013**, *169*, 137−147. (b) Chebbi, M.; Azambre, B.; Cantrel, L.; Koch, A. A Combined Drifts and DR−UV−VIS Spectroscopic in Situ Study on the Trapping of CH_3I by Silver−Exchanged Faujasite Zeolite. *J. Phys. Chem. C* **2016**, *120* (33), 18694−18706.

(20) Santillán, J. M.; Muñetón Arboleda, D.; Muraca, D.; Schinca, D. C.; Scaffardi, L. B. Highly Fluorescent Few Atoms Silver Nanoclusters with Strong Photocatalytic Activity Synthesized by Ultrashort Light Pulses. *Sci. Rep.* **2020**, *10* (1), 8217.

(21) Bartolomeu, R.; Azambre, B.; Westermann, A.; Fernandes, A.; Bertolo, R.; Hamoud, H. I.; Henriques, C.; Da Costa, P.; Ribeiro, F. Investigation of the Nature of Silver Species on Different Ag−Containing NO_x Reduction Catalysts: On the Effect of the Support. *Appl. Catal. B: Environ.* **2014**, *150*, 204−217.

(22) Sandoval, A.; Delannoy, L.; Methivier, C.; Louis, C.; Zanella, R. Synergetic Effect in Bimetallic Au−Ag/TiO_2 Catalysts for CO Oxidation: New Insights from in Situ Characterization. *Appl. Catal. A: Gen.* **2015**, *504*, 287−294.

(23) Hadjiivanov, K. Chapter Two − Identification and Characterization of Surface Hydroxyl Groups by Infrared Spectroscopy. In *Advances in Catalysis*; Jentoft, F. C., Ed.; Academic Press, 2014; Vol. *57*; pp 99−318.

(24) Müslehiddinoğlu, J.; Vannice, M. A. CO Adsorption on Supported and Promoted Ag Epoxidation Catalysts. *J. Catal.* **2003**, *213* (2), 305−320.

(25) (a) Komine, N.; Flores, J. A.; Pal, K.; Caulton, K. G.; Mindiola, D. J. Büchner Reactions Catalyzed by a Silver (I) Pyridylpyrrolide: Understanding Arene C−C Insertion Selectivity. *Organometallics* **2013**, *32* (11), 3185−3191. (b) Fortea-Pérez, F. R.; Mon, M.; Ferrando-Soria, J.; Boronat, M.; Leyva-Pérez, A.; Corma, A.; Herrera, J. M.; Osadchii, D.; Gascon, J.; Armentano, D. The MOF−Driven Synthesis of Supported Palladium Clusters with Catalytic Activity for Carbene−Mediated Chemistry. *Nat. Mater.* **2017**, *16* (7), 760−766.

(26) Zhao, J.; Ji, S.; Guo, C.; Li, H.; Dong, J.; Guo, P.; Wang, D.; Li, Y.; Toste, F. D. A Heterogeneous Iridium Single−Atom−Site Catalyst for Highly Regioselective Carbenoid O−H Bond Insertion. *Nat. Catal.* **2021**, *4* (6), 523−531.

(27) Corma, A.; Garcia, H.; Leyva, A. Controlling the Softness−Hardness of Pd by Strong Metal−Zeolite Interaction: Cyclisation of Diallylmalonate as a Test Reaction. *J. Catal.* **2004**, *225* (2), 350−358.

(28) Oudenhuijzen, M. K.; van Bokhoven, J. A.; Miller, J. T.; Ramaker, D. E.; Koningsberger, D. C. Three−Site Model for Hydrogen Adsorption on Supported Platinum Particles: Influence of Support Ionicity and Particle Size on the Hydrogen Coverage. *J. Am. Chem. Soc.* **2005**, *127* (5), 1530−1540.

(29) (a) Dempsey, E. Calculation of Madelung Potentials for Faujasite−Type Zeolites. I. *J. Phys. Chem.* **1969**, *73* (11), 3660−3668. (b) Ferenczy, G. G.; Ángyán, J. G. Calculations on Electrostatic Properties of HY Zeolite. *J. Chem. Soc., Faraday Trans.* **1990**, *86* (20), 3461−3466.

(30) (a) Areán, C. O.; Palomino, G. T.; Zecchina, A.; Spoto, G.; Bordiga, S.; Roy, P. Cation−Carbon Stretching Vibration of Adducts Formed Upon CO Adsorption on Alkaline Zeolites. *Phys. Chem. Chem. Phys.* **1999**, *1* (17), 4139−4140. (b) Concepcion-Heydorn, P.; Jia, C.; Herein, D.; Pfänder, N.; Karge, H. G.; Jentoft, F. C. Structural and Catalytic Properties of Sodium and Cesium Exchanged X and Y Zeolites, and Germanium−Substituted X Zeolite. *J. Mol. Catal. A: Chem.* **2000**, *162* (1−2), 227−246.

(31) Huang, M.; Adnot, A.; Kaliaguine, S. Characterization of Basicity in Alkaline Cation Faujasite Zeolites−an XPS Study Using Pyrrole as a Probe Molecule. *J. Catal.* **1992**, *137* (2), 322−332.

(32) Porto, V.; Buceta, D.; Domínguez, B.; Carneiro, C.; Borrajo, E.; Fraile, M.; Davila-Ferreira, N.; Arias, I. R.; Blanco, J. M.; Blanco, M. C.; Devida, J. M.; Giovanetti, L. J.; Requejo, F. G.; Hernández-Garrido, J. C.; Calvino, J. J.; López-Haro, M.; Barone, G.; James, A. M.; García-Caballero, T.; González-Castaño, D. M.; Treder, M.; Huber, W.; Vidal, A.; Murphy, M. P.; López-Quintela, M. A.; Domínguez, F. Silver Clusters of Five Atoms as Highly Selective Antitumoral Agents Through Irreversible Oxidation of Thiols. *Adv. Funct. Mater.* **2022**, *32* (29), 2113028.

(33) (a) Ranocchiari, M.; Mezzetti, A. Ru/PNNP−Catalyzed Asymmetric Imine Aziridination by Diazo Ester Activation. *Organometallics* **2009**, *28* (13), 3611−3613. (b) Albertin, G.; Antoniutti, S.; Botter, A.; Castro, J. Hydrolysis of Coordinated Diazoalkanes to Yield Side−On 1, 2−Diazene Derivatives. *Inorg. Chem.* **2015**, *54* (5), 2091−2093.

(34) Pujol, A.; Lafage, M.; Rekhroukh, F.; Saffon-Merceron, N.; Amgoune, A.; Bourissou, D.; Nebra, N.; Fustier-Boutignon, M.; Mézailles, N. A Nucleophilic Gold(III) Carbene Complex. *Angew. Chem., Int. Ed.* **2017**, *56* (40), 12264−12267.

(35) (a) Tyo, E. C.; Vajda, S. Catalysis by Clusters with Precise Numbers of Atoms. *Nat. Nanotechnol.* **2015**, *10* (7), 577−588. (b) Malola, S.; Häkkinen, H. Prospects and Challenges for Computer Simulations of Monolayer−Protected Metal Clusters. *Nat. Commun.* **2021**, *12* (1), 2197. (c) Zaker, Y.; Ashenfelter, B. A.; Bhattarai, B.; Diemler, N. A.; Brewer, T. R.; Bigioni, T. P. Sequential Growth as a Mechanism of Silver−Glutathione Monolayer−Protected Cluster Formation. *Small* **2021**, *17* (27), 2002238. (d) Dong, C.; Gao, Z.; Li, Y.; Peng, M.; Wang, M.; Xu, Y.; Li, C.; Xu, M.; Deng, Y.; Qin, X.;

https://doi.org/10.1021/jacs.3c08317
J. Am. Chem. Soc. 2023, 145, 24736−24745

et al. Fully Exposed Palladium Cluster Catalysts Enable Hydrogen Production from Nitrogen Heterocycles. *Nat. Catal.* **2022**, *5* (6), 485−493.

(36) Liu, L.; Corma, A. Confining Isolated Atoms and Clusters in Crystalline Porous Materials for Catalysis. *Nat. Rev. Mater.* **2021**, *6* (3), 244−263. (b) Liu, L.; Lopez-Haro, M.; Perez-Omil, J. A.; Boronat, M.; Calvino, J. J.; Corma, A. Direct Assessment of Confinement Effect in Zeolite−Encapsulated Subnanometric Metal Species. *Nat. Commun.* **2022**, *13* (1), 821.

https://doi.org/10.1021/jacs.3c08317
J. Am. Chem. Soc. 2023, 145, 24736−24745